MODELS FOR OBTAINING EFFECTS OF GROUND WINDS ON SPACE VEHICLES ERECTED ON THE LAUNCH PAD

by

Wilmer H. Reed, III

NASA - Langley Research Center

ABSTRACT

The paper describes how, through simulation with physical and mathematical models, the effects of ground winds on erected launch vehicles are being studied at the NASA, Langley Research Center. Experimental programs include both aeroelastically scaled models in wind tunnels and full-scale vehicles in natural winds. With the aid of a mathematical model having nonlinear aerodynamic damping, insight is gained which helps explain why in some instances the response at supercritical Reynolds numbers is a result of random forced excitation while in other instances is characterized by a self-excited periodic motion.

Consideration is also given to the response of erected vehicles to atmospheric turbulence. It is shown that at the fundamental cantilever frequency of Saturn V class vehicles the gust velocities along the vehicle

are essentially uncorrelated for separation distances greater than a few vehicle diameters. Calculations indicate that the response is significantly reduced when these spatial correlations of gusts are taken into account.

INTRODUCTION

This paper will concern a search for new solutions to an old problem; namely, the effect of wind loads on flexible bluff bodies. For years civil engineers have grappled with the problem in the design of such structures as smoke stacks, suspension bridges, and tall masts. (See, for example, refs. 1 through 4). I should point that included in these studies are contributions by the Director of this Conference, Professor Maher, who has conducted extensive wind-tunnel tests of suspension bridge section models. (See, for example, ref. 2.)

Starting with Goldman's investigation of ground-wind loads for the Vanguard in 1957 (ref.5), some form of wind-tunnel tests relating to this problem has been a part of the development program for practically every launch vehicle. Examples of such studies on specific vehicles are to be found in references 6 through 9, and other more general studies of vortex shedding from cylindrical bodies are given in references 10 through 13. We find further evidence of the extent of effort presently being expended in this area by noting that at the annual AIAA Conference on Structures and Materials held at Palm Springs, California in April of this year, five out of a total of seventeen papers in sessions on structural dynamics concerned the subject of vortex shedding from bodies of revolution. Despite this extensive research, there remain many important

questions to be answered, especially in the high Reynolds number range.

With the aid of figure 1 let us identify the primary ingredients of the problem at hand. This schematic diagram shows a launch vehicle on a flexible support structure standing beside an umbilical tower. A steady wind imposes both static and dynamic loads on the vehicle. The static loads act primarily in the direction of the mean wind and the dynamic loads, which are associated with vortices shed from the vehicle, are largest in the direction perpendicular to the wind. These dynamic loads, which may result from either a random forced response or a periodic self-excited response, are frequently several times greater than the static drag loads. The adjacent tower structure and its turbulent wake may also have an influence on wind loads. These wind loads create problems in structural strength, guidance alinement, and clearance between adjacent structures.

The purpose of this paper will be to discuss recent studies in the area of ground-wind loads being conducted at the Langley Research Center. In particular, we will consider four items: wind-tunnel models and test techniques, self-excited response, effects of atmospheric turbulence, and full-scale programs.

WIND-TUNNEL MODELS AND TEST TECHNIQUES

Aeroelastic Models

The aerodynamic forces associated with ground-wind loads on erected launch vehicles are a result of flow separation from bluff bodies. Since such loads are critically dependent on Reynolds number, efforts are made to duplicate full-scale Reynolds numbers in the wind tunnel. Also, because of the sensitivity of flow separation to minor surface protuberances, such as conduits or surface roughness conditions, careful attention must be given to the simulation of detailed geometric features. If steady-state loads were the only consideration, a rigid model having the same geometric features and Reynolds numbers as the prototype would be adequate for predicting ground-wind loads. Unfortunately, launch vehicles are not rigid and usually the predominant aerodynamic loads are not steady. Therefore, the structural dynamic properties of the vehicle, that is, mass, frequency, and damping, also become important considerations in model scaling. Experience has shown that the predominant dynamic response of launch vehicles to wind-induced loads is essentially that of the first mode alone. The significant additional nondimensional parameters to be matched in the wind tunnel are then the reduced frequency based on the fundamental frequency of the vehicle $\omega_1 D/U$, the structural damping, and a mass ratio involving generalized mass of the fundamental mode to the mass of air displaced by the vehicle.

A model which simulates both aerodynamic and structural dynamic parameters is referred to as an "aeroelastic" model. Wind-tunnel tests of such models are believed to provide the most direct and realiable means of predicting the response of launch vehicles to a steady wind. (See, for

example, refs. 14 and 15).

Shown in figure 2 are some aeroelastic models of specific vehicles which have been used in ground-wind-load studies in the Langley 16-foot transonic dynamics tunnel during the past 4 years. Notice that in most instances the vehicle models are tested in the presence of simulated umbilical towers or service structure. These towers are usually scaled only with regard to over-all geometry. The exception is the erector tower for the Titan-Gemini which had scaled frequencies. The models - vehicle and tower structures - are installed on a remotely controlled turntable so as to permit response measurements to be taken from any wind direction.

By using a freon test medium, which has a kinematic viscosity of about one-fifth that of air, Reynolds number simulation can be approximately achieved for all of the vehicles shown except for the Saturn V. For this model, which is 3 percent of full-scale size, the Reynolds number in the wind tunnel was one-third of the full-scale value.

Even when Reynolds number is matched, however, there are differences in the flow in wind tunnels as compared with that in the natural atmosphere. In the wind tunnel the flow is approximately uniform and steady; in the atmosphere near the ground the mean wind varies with height and is gusty. An approximate means of taking into account wind variations with height is to relate the wind-tunnel velocity to a calculated "equivalent" velocity which produces the same steady-state base-bending moment as does the actual wind profile. A reasonable approximation of natural wind profiles has been simulated in wind tunnels by use of a transverse grid of various sized rods. (See refs. 16 and 17.) A pilot study is presently underway at Langley to determine the feasibility of applying these techniques in ground-wind load studies.

Modeling criteria for simulating atmospheric turbulence in wind tunnels have also been successfully applied in reference 18. These scaling laws, however, are not compatible with those used in the scaling of aeroelastic models. Some further consideration of the scaling of natural turbulence in wind tunnels will be given in a later section of this paper.

Response Measurements

The principal response measurements in these studies are the static and dynamic bending moments in two planes at the base of the model, and corresponding accelerations at the nose. Although time histories of the quantities are recorded, the most useful readout system employed in a two-axis oscilloscope and camera. As illustrated in figure 3, the outputs of X and Y bending-moment strain gages are fed to the X and Y axes of the scope and the sensitivities of the two channels are made equal. A time-exposure photograph of the oscillograph screen produces a roughly elliptical pattern which defines the envelope of the maximum bending-moment oscillations encountered during the data sampling period; typically, the model encounters between 2,000 and 3,000 cycles of oscillation during this period, which, in terms of the full-scale vehicle, is equivalent to wind exposure times of the order of 1 hour. The vector from the wind-off point to the center of the elliptical pattern represents the static moment, and the longest vector which can be drawn from the wind-off point to the tangent on the ellipse is the maximum resultant moment. Note that information on the correlation between the two-moment time histories is displayed with this type of data presentation. It has been found that the probability of the lateral and dragwise bending moments reaching maximum values at the same time is very low.

Damping Devices

Structural damping has been found to be one of the key parameters which governs the susceptibility of a vehicle to wind-induced oscillations. It is very difficult, however to control damping in a model as accurately as other parameters. A viscous damper, shown in figure 4, has been developed which permits precise regulation of the damping in a model. The device works on the principle of the classical Lanchester damper. It consists of a series of lead slugs (auxiliary masses) that are free to slide on concave trays inside of a cylinder filled with viscous oil. As the cylinder vibrates in a horizontal plane, the oil moves relative to the slugs, thereby causing energy to be dissipated. The damping can be varied by changing the number of slugs or the viscosity of the oil. Figure 5 shows the increase in damping in the 0.03-scale Saturn V model obtained with eight 72-gram slugs in the damper.

Various damping devices have been used or proposed as means of alleviating wind-induced oscillations of smoke stacks. Usually the dampers are connected to the structure by means of guy wires (ref. 3 and 4). Since guy wire supports are often not feasible in launch vehicle applications, it is of interest to consider the use of auxiliary mass dampers, which requires no external connections, as a possible method for reducing wind-induced loads on full-scale vehicles. Such devices presumably could be attached to the vehicle during high wind conditions and then be removed prior to launch.

Theoretical performance characteristics of an auxiliary mass damper are shown in figure 6 as a three-dimensional surface. It is assumed that an auxiliary mass m is connected to the vehicle structure through a spring k_d and dashpot c, as indicated schematically in the figure. The

vehicle structure is represented mathematically as a single-degree-of freedom oscillator having a generalized mass M and natural frequency ω_1. The case shown is for $m/M = 0.05$. The vertical axis in the figure is the damping ratio ζ_1 associated with the vehicle mode; this was determined from the real part of one root of the characteristic equation for the coupled system. Plotted on the other axes are ω_d/ω_1, the ratio of uncoupled frequencies, and $c/2m\omega_1$, a nondimensional viscous damping parameter. This figure simply illustrates a well-known result from the theory of vibration absorbers (see, for example, ref. 19) that when the auxiliary mass is "tuned" to the natural frequency of the system to which it is attached, and $c/2m\omega_1$ is near an optimum value, large energy dissipation can be achieved. The previously discussed Lanchester type damper is represented by the curve for $\omega_d/\omega_1 = 0$. Note that this damper has optimum performance at $c/2m\omega_1 = 0.5$. The wind-tunnel research applications where precise control of damping in aeroelastic models is desired, the fact that ζ_1 is relatively insensitive to variations in $c/2m\omega_1$ becomes an attractive feature; however, in full-scale applications, where weight of the auxiliary mass may be an important consideration, tuned dampers offer more than an order of magnitude improvement in performance.

SELF-EXCITED RESPONSE

Various and conflicting theories have been advanced regarding unsteady aerodynamic forces associated with vortex shedding from circular cylinders. In the supercritical Reynolds number range - the range of primary interest for the present problem - experimental data indicate that in some instances these forces are random and insensitive to motion of the structure (Fung,

ref. 10) and in other instances periodic and strongly dependent on motion (Buel, et al., ref. 12 and Den Hartog, ref. 3). This section of the paper will be devoted to consideration of these apparent differences. In particular, a simple mathematical model, involving nonlinear aerodynamic damping, is presented which has behavior consistent with both of the above-mentioned phenomena.

Experimental Results

In recent wind-tunnel tests at Langley involving Saturn I-B and Saturn V ground-wind load models violent self-excited oscillations were encountered. These oscillations occurred at Reynolds numbers as high as 4×10^6 based on the model's maximum diameter. On both models the instability appeared at reduced frequencies, based on the maximum diameter, in the neighborhood of 0.2 which happens to be the Strouhal number of the Karman vortex street at subcritical Reynolds number.[1] Similar self-excited response phenomena have been observed on large, lightly damped, steel smokestacks and the solution has been to add damping (ref. 3) or attach aerodynamic spoilers to the structure (ref. 20).

Now it might be argued that these high response conditions observed at a particular wind velocity could be in the nature of a forced resonant oscillation rather than an instability. Data presented in figure 7, however,

---

[1] It should be noted that for these models the peak response appears to be a result of vortex shedding from the lower stages at a Strouhal number of 0.2. Response characteristics were relatively insensitive to changes in nose shape or surface roughness conditions; for other vehicles configurations, nose shape and roughness may be the dominant factor affecting response. (See ref. 12.)

serve to disprove this argument. These data were obtained on the 0.03-scale Saturn V model. The figure shows the variation of dynamic bending-moment response with velocity for three values of structural damping. First, note that for the smallest damping of $\zeta = 0.004$, the response peaks sharply at a reduced velocity of approximately 4.5. The sample time history shown for the peak response point is a nearly constant amplitude sine wave at the fundamental model frequency. When the damping is increased from 0.004 to 0.008 the sharp spike is eliminated and the response time history is characterized by a random-amplitude constant-frequency motion typical of the response of a lightly damped system to a random-forcing function. This complete change in character of the response time histories as damping increases suggests that at a certain critical velocity the structural damping of the system is a controlling factor which determines whether the dynamic response is a result of self-excited or externally forced motions. In either case it is apparent that structural damping of the model is an important parameter to be simulated. Furthermore, the commonly used scaling laws (ref. 21) based on the response of systems to random or periodic forcing functions, without consideration of motion-dependent aerodynamic forces, would be inapplicable for these cases of self-excited response. Similar results are shown in reference 12.

Conceptual Model of Self-Excited Response

Let us now attempt to interpret the mechanism producing these observed dynamic instabilities. Scruton, in reference 22, has made extensive wind-tunnel studies of industrial structures such as smokestacks and towers, and has reported similar instabilities which he attributes to a nonlinear aerodynamic damping that becomes negative at a particular wind velocity. Scruton's results were obtained at subcritical Reynolds numbers; however, his findings

appear to be applicable to the present studies where Reynolds number varies from 1 to 6 million.

A launch vehicle structure and the aerodynamic loads associated with vortex shedding are represented conceptually by the block diagram pictured in figure 8. Let $F_S(t)$ be the aerodynamic forcing function which is independent of vehicle motion and $F_D(t)$ to a nonlinear aerodynamic damping force which depends on the vehicle motion. In the equations of motion, also given in figure 8, the left-hand side describes dynamics of the structure in terms of a natural frequency and damping ratio and the right-hand side expresses the aerodynamic forces in terms of a lateral force coefficient $C_L(t)$ and damping coefficient $C_{\dot{x}}$. For the present purpose it will be assumed that $C_L(t)$ is a random function of time. Depending on the relative magnitudes of the structural and the aerodynamic damping coefficients, the response $x(t)$ of the structure in the direction perpendicular to the wind can take on either of the two forms indicated in the figure. When the damping is predominantly structural, the response will be the characteristic random-amplitude constant-frequency motion typical of a lightly damped system driven by a random forcing function. With aerodynamic damping present in a nonlinear form such as measured by Scruton, the possibility exists for self-excited motions indicated in the figure by the constant amplitude sinusoidal response. A representative plot of the variation of $C_{\dot{x}}$ with reduced frequency (see fig. 9) shows that over a narrow range of fD/U near 0.20, the aerodynamic damping has a destabilizing influence which depends strongly on the amplitude of motion. At this critical value of reduced frequency the destabilizing effect becomes smaller as the amplitude of motion increases. Thus, an energy balance is eventually established between the energy input by negative aerodynamic damping and the energy absorbed by positive

structural damping. This leads to a limit-cycle oscillation whose amplitude is inversely proportional to structural damping as shown in plot on right side of figure 9.

Analog Computer Studies

Further insight into the behavior of the nonlinear mathematical model presented in figures 8 and 9 may be gained from analog computer solutions. For this purpose the equation in figure 9 has been programmed on an analog computer in the manner shown in figure 10. The random lateral forcing function $C_L(t)$ was obtained by passing the output of a Gaussian white-noise generator through a first-order low-pass filter. The filter time constant was adjusted to make the power spectrum of $C_L(t)$ approximate closely the spectrum for fixed cylinders presented by Fung in figure 11 of reference 10. Output of the noise generator was adjusted such that the root-mean-square of C_L matched Fung's measured value of 0.12. As an approximation to Scruton's results in reference 22, the nonlinear damping coefficient was assumed to be inversely proportional to a running average of the absolute value of response.

The results are shown in figure 11 as a plot of maximum response observed during a computer run against damping of the structure. The plot on the left of the figure represents the system response with the motion-dependent aerodynamic force set equal to zero. This response varies inversely as $\sqrt{\zeta}$ which is the relationship predicted for lightly damped systems acted on by a random forcing function. (See ref. 21.) According to Scruton's data this is representative of conditions when the natural frequency of the system is not in the vicinity of the Strouhal frequency. The right-hand side of the figure shows corresponding results when the natural frequency and the Strouhal frequency have approximately the same

values, say, $f_n D/U \approx 0.2$. Note the similarities in these analog time histories and the bending-moment time histories shown in figure 7 for the Saturn V model.

The apparent inconsistencies between Fung's observation (ref. 10) - aerodynamic forces on cylinders are random and essentially independent of body motions - and the self-excited response observed for both wind-tunnel models and smokestacks might then be reconciled as follows: In Fung's investigation, the cylinder motion was limited to reduce frequencies below 0.12; Scruton (ref. 22) and the present wind-tunnel studies indicate that motion dependent forces, in the form of negative aerodynamic damping occur in a narrow range of reduced frequencies near the Strouhal number of 0.2. In order to shed further light on these and related questions, a generalized research study on two-dimensional cylinders will be conducted in the Langley transonic dynamics tunnel up to Reynolds number of 20×10^6. The Martin Company, George C. Marshall Space Flight Center, and Langley Research Center will be joint participants in this program.

RESPONSE TO TURBULENCE

Comparison of Wind-Tunnel and Atmospheric Turbulence

Unlike the uniform profile of steady wind in a wind tunnel, atmospheric winds near the ground are typically as illustrated in figure 12. The profile patterns shown represent instantaneous distributions of horizontal wind that may occur as a field of turbulence is blown past an erected vehicle. The dashed line in the figure represents the mean wind averaged over, say, a 1-minute period; the little arrows represent more rapid wind fluctuations of wind components in the direction of the mean flow. As indicated in the figure, these unsteady wind components vary randomly in both time and space. Since

these winds produce random loadings on the structure, power spectral techniques appear to offer the most fruitful method of analysis and will be the approach discussed in the present paper.

Before considering some mathematical techniques for predicting the response of launch vehicles to ground wind turbulence, let us first discuss the possibility of simulating such turbulence in a wind tunnel. Consider the question: To what extent would the turbulence structure representative of wind tunnels need to be modified in order to simulate "atmospheric" turbulence in wind-tunnel testing of aeroelastically scaled models? Figure 13 will serve to answer this question. The figure shows typical plots of the power spectrum of wind-tunnel turbulence and atmospheric turbulence near the ground. The curves are plotted against the familiar frequency scaling parameter fD/U. Turbulence, whether it be in the earth's boundary layer or in a wind tunnel, can be characterized by a mean eddy size or "scale" length L, and the rms intensity of fluctuation components relative to the mean wind velocity, $\sqrt{u^2}/U$. For atmospheric winds near the ground, the scale of turbulence is of the order of the over-all length of Saturn V vehicle, or 10 vehicle diameters. In wind tunnels a typical value of L might be 1/10 the diameter of a ground-wind-loads model. Also, the intensity of turbulence is an order of magnitude different for the two cases, being, say, 20 percent of the mean wind for the atmosphere as compared with 1 or 2 percent for wind tunnels. In summary, the figure indicates that over the frequency range of interest in the present problem, typical values of the scale and intensity of turbulence in wind tunnels and in the atmosphere are vastly different; therefore, study of the effects of gust loads associated with atmospheric turbulence in wind tunnels must await the development of new techniques for the generation and control of wind-tunnel turbulence.

Basic Power Spectral Relationships

In absence of suitable wind-tunnel techniques for studying the response of vehicles to atmospheric turbulence, we must work either with mathematical models or actual structures exposed to natural winds. Both of these approaches are being pursued at NASA-Langley. This section of the paper will concern an analytical approach to the problem.

Power spectral techniques have proved to be powerful tools for analyzing the response of systems to random inputs. Such techniques for aircraft gust-load prediction have been under development for more than a decade and offer an excellent foundation on which to formulate the present problem. Of particular value is the paper by Houbolt, Steiner, and Pratt (ref. 23) which presents an exhaustive review and extension of power spectral techniques in relation to the response of airplanes to atmospheric turbulence. A basic equation for the power spectrum of a linear system acted upon by multiple random inputs is presented in references 23 and 24 wherein the structure is assumed to be divided into an arbitrary number of segmented areas with a random forcing function acting at the center of each segment.

$$\Phi_r(\omega) = \Phi_{11}H_1H_1^* + \Phi_{22}H_2H_2^* + \Phi_{33}H_3H_3^* + \ldots$$

$$+ 2R_e(\Phi_{12}H_1^*H_2 + \Phi_{13}H_1^*H_3 + \ldots\Phi_{23}H_2^*H_3 + \ldots) \qquad (1)$$

where

$\Phi_r(\omega)$ power spectrum of a response variable r which may denote base bending moment, tip deflection, etc.

Φ_{ij} cross spectrum of turbulence velocities at i^{th} and j^{th} points on the structure

H_i frequency response function which gives the response due to a unit sinusoidal gust component velocity acting at the segment of surface area associated with the i^{th} point

$H_i^*(\omega) = H_i(-\omega)$ complex conjugate of H_i

Re denotes the real part

In its general form this equation indicates that a considerable amount of information regarding the spectral description of turbulence is required in order to define the response spectrum. Specifically, the power spectrum of horizontal components of turbulence must be specified as a function of frequency at each of n points on the structure together with the cross spectra between all combinations of pairs of the velocity components. Since such information is rarely available in the form required, various simplifying assumptions must be made in order to obtain numberical solutions to equation (1). The most frequently made assumptions are that the gust velocities are in phase at every point on the structure and that the turbulence field is homogeneous; that is,

$$\Phi_{11} = \Phi_{12} = \Phi_{13} \cdots \Phi_{1n} \tag{2}$$

With these assumptions, equation (1) reduces to the following simple form

$$\Phi_r(\omega) = |H|^2 \Phi_{11} \tag{3}$$

where

$H = H_1 + H_2 + \ldots H_n$ frequency response function for a sinusoidal gust uniformly distributed over the vehicle length

Φ_{11} power spectrum of gust components

Bohne, in reference 25, utilizes this equation in analyzing the response of launch vehicles to ground-wind turbulence. Various empirical expressions

for the power spectrum of turbulence, derived from data obtained from wind towers and airplanes, are available for use in such calculations. (See, for example, refs. 23, 26, 27, and 28.)

An obvious shortcoming of the assumption of perfect correlation of gusts along the length is that dynamic response in the fundamental mode is likely to be grossly overestimated, especially if gust wave lengths corresponding to the fundamental structural frequency are small in comparison with the vehicle length. A more rational assumption would be to account for correlation of gust velocities on the basis that atmospheric turbulence is locally homogeneous and isotropic; that is, its statistical properties in a given volume of air are the same at all points and are independent of rotations of the reference axes. In an analysis of response of line-like structures to gusty winds, Davenport (ref. 29) makes similar assumptions and justifies them on the basis of experimental evidence. Under these conditions the cross spectra depend only on the separation distance between points and are independent of height above the ground. The following relations then apply

$$\Phi_{11} = \Phi_{22} = \Phi_{33} = \cdots \Phi_{nn}$$

$$\Phi_{12} = \Phi_{23} = \Phi_{34} = \cdots \Phi_{n,n+1}$$

$$\Phi_{13} = \Phi_{24} = \Phi_{35} = \cdots \Phi_{n,n+2} \qquad (4)$$

and equation (1) becomes

$$\Phi_r(\omega) = \Phi_{11} \left\{ H_1 H_1^* + H_2 H_2^* + \cdots 2\mathrm{Re} \left[\frac{\Phi_{12}}{\Phi_{11}} (H_1^* H_2 + H_2^* H_3 + \ldots) \right.\right.$$

$$\left.\left. + \frac{\Phi_{13}}{\Phi_{11}} (H_1^* H_3 + H_2^* H_4 + \ldots) + \frac{\Phi_{1n}}{\Phi_{11}} (H_1^* H_n + H_2 H_{n+1} + \ldots) \right] \right\} \qquad (5)$$

Cross Spectra of Turbulence

In order to calculate the response spectrum on the basis of equation (5) the cross-spectra functions must first be specified. These functions are derived in appendix A from theoretical considerations which employ Taylor's hypothesis (i.e., fixed patterns of turbulence are transported at the mean wind velocity) together with the assumption that over the height intervals of interest the turbulence is homogeneous and isotropic. Results from the theory are plotted in figure 16. Also shown in figure 15(a) are experimental data obtained by Singer (ref. 30) from a 400-foot tower in wooded country at the Brookhaven Laboratory and by Davenport (ref. 29) on a 500-foot mast in open grassland. It is encouraging to note that the experimental data from both of these sites are in reasonable agreement and that the theoretical curve falls within the scatter of the data.

Probably the most significant feature of figure 15 is that for vertical separation distances greater than about 0.3 of u component wavelengths or 0.5 of v component wavelengths the gusts are essentially uncorrelated. For example, in a 60-knot wind at a frequency corresponding to the Saturn V fundamental cantilever frequency (f 0.5 cps), correlation of u gust components is negligible for separation distances greater than two maximum-vehicle diameters.

The ordinate in figure 15, defined as the square root of the coherency function, represents the modulus of the complex cross spectra which consists of a real (copower) part and an imaginary (quadpower) part. It should be pointed out that in the theoretical cross spectra the quadpower is zero whereas in the experimental cross spectra a small quadrature component was measured. These quadrature components are due in part to shear flow in the wind profile and also probably lags in the wind sensors.

Applications

In appendix B the frequency response functions indicated in equation (5) are derived in terms of natural vibration modes of a structure. The response spectrum for a two-dimensional gust input is then expressed as a product between the response spectrum for one-dimensional gusts and a so-called "attenuation" factor which accounts for the two-dimensionality of turbulence. For example, the spectrum of response in the x direction due to u gust components is (see eq. (B-15a)

$$\Phi_x(k) = T_{un}(k)\Phi_x(k)_{,uniform}$$

where the subscript n refers to the mode number and $T_{un}(k)$ is the attenuation factor given by equation (B-16) in appendix B. Examination of this matrix equation indicates that $T_{un}(k)$ is dependent on such factors as vehicle geometry, mode shape, wind profile shape, and the cross spectra of turbulence between points along the vehicle.

In order to present some specific results the gust attenuation factor $T_{un}(k) = \Phi_x/\Phi_{x,uniform}$ was evaluated for a Saturn V class vehicle in a cantilevered unfueled condition. The Saturn V has a maximum diameter of 33 feet and is about 350 feet tall. Natural frequencies of the first two cantilevered modes were assumed to be 0.48 cps and 1.85 cps. The steady wind profile shape considered followed a 1/5 power law variation with height as suggested in reference 31.

Results of these calculations are presented in figure 16. Note that for reduced frequencies fD/U greater than about 0.1 attenuation due to two-dimensional effects is approximately twice as great for the first mode as it is for the second mode. A physical explanation of this result can be gained by recognizing that in the first mode a 180° phase shift for gusts on opposite

sides of the node line has a load amplifying effect. Similar results are noted in reference 24.

Although gust correlation effects tend to attenuate the first mode to a much greater extent than the second mode, the absolute response is, nevertheless, predominantly that of the first mode. This result is associated with the rapid decrease in turbulent energy with increasing frequency.

An interesting feature to be noted is that the curves in figure 16 are independent of the scale of turbulence. This is a consequence of the assumption made in appendix A that the gust wavelengths of interest are equal to or less than the scale of turbulence.

Power spectra of first-mode response to u and v gust components are presented in figure 17 for 1-D and 2-D turbulence. The response deflection has been made nondimensional by dividing it by the static deflection associated with the mean wind speed. In these calculations it has been assumed that the wind speed is the 99.9 percent probable maximum at Cape Kennedy (ref.31) which is 43.4 knots at the 240-foot height. The velocity at this height is the effective wind velocity U_e which, if distributed uniformly over the vehicle, would produce the same static dragwise base bending moment as does the assumed wind profile. The mean square turbulence was assumed to be $\bar{u}^2 = \bar{v}^2 = 0.03\ U_e^2$. And finally, the form of the power spectra for u and v was assumed to be given by equation (B-14) with $L = 10D_0 =$ 330 ft at all heights.

Note in the figure that at the lower frequencies, corresponding to long wavelengths, the 1-D and 2-D response curves are almost identical. In the vicinity of the first-mode natural frequency, however, the effects of 2-D turbulence are indeed significant. From areas under the spectra curves the variance of response for 1-D gusts are approximately twice that of the 2-D gusts.

FULL-SCALE STUDIES

In previous sections of the paper we have discussed ways in which the response of launch vehicles to ground-wind loads can be simulated by means of models - both physical and mathematical. Whether or not these models are the intended analogs of their full-scale counterparts must be judged on the basis of comparisons between appropriate model and full-scale data. Although considerable effort has been devoted to wind-tunnel studies of aeroelastic ground-wind models, there is little in the way of full-scale data available for correlation with similar model data.

Jupiter and Thor Vehicles

In order to fill this gap the Langley Research Center is engaged in two programs aimed at obtaining ground-wind response data on full-scale vehicles. The first of these programs involves use of a Jupiter and a Thor vehicle which have been acquired as surplus property. These vehicles are to be used solely for ground-wind-load studies over a 1-year period at Wallops Island. Vehicle response, in the form of bending moments and accelerations, will be measured together with the wind inputs at two heights near each vehicle. In addition, other wind measurements will also be obtained from five elevations on a 250-foot tower located about 1/4 mile from the vehicle site. Special fast-response anemometers similar to the prototype shown in figure 18 (ref. 32) will be used. These instruments have flat response to frequencies several times greater than the fundamental vehicle frequencies. Vehicle response and wind input data will be automatically recorded on magnetic tape at regular intervals, or whenever the wind exceeds a preselected value.

The previously mentioned wind-tunnel tests of a 20-percent scale Jupiter model indicated that small strake-type spoilers placed on the nose had a pronounced load alleviation effect. These results are shown in figure 19 as a plot of the maximum resultant bending moment against wind speed. One of our first objectives in the full-scale program, then, will be to determine if spoilers are in fact as effective as predicted in the wind-tunnel studies.

Titan-Gemini

The second full-scale ground wind response program has been established for the Titan-Gemini at Cape Kennedy. This program is being conducted by Martin-Baltimore under contract with the Air Force and Manned Spacecraft Center. It will be closely followed by the Langley Research Center while, in addition to having conducted wind-tunnel studies of the vehicle and erector system, is providing the previously mentioned fast-response anemomenters for the wind-measurement phase of the program. The bending-moment response of the vehicle will be read out from load cells which are a part of the launch pad hold-down structure. For each vehicle there will be two opportunities to obtain response data when the vehicle is not sheltered by the erector tower; these are during a fuel loading checkout and immediately prior to launch.

Although the system is not yet fully operational, some bending-moment response data were obtained by the Martin Company just prior to launch of the first Titan-Gemini vehicle. These data are presented in figure 20 together with wind-tunnel results and theoretical predictions of response due to turbulence. The only source of wind data available at the time of these measurements was a propeller-type anemometer mounted a few feet above the blockhouse and read out visually on a meter. Therefore, precise values

for the mean wind and the intensity of turbulence at the vehicle are not known; the intensity of turbulence assumed in these calculations was $\sqrt{u^2}/U = \sqrt{v^2}/U = 0.2$. Although there appears to be reasonable agreement indicated between these full-scale measurements and the predictions based on wind-tunnel data and assumed turbulence conditions, quantitative comparisons should not be attempted until the more precise measurements of the wind are available.

CONCLUDING REMARKS

This paper concerns the role simulation plays in prediction of effects of ground winds on space vehicles erected on the launch pad. It is shown that with present techniques, both wind-tunnel and mathematical models are required in order to predict the response of vehicles to gusty winds. By means of a conceptual representation, which involves a random forcing function and nonlinear aerodynamic damping, new insight is gained into the mechanism of self-excited response which has been observed at supercritical as well as subcritical Reynolds numbers. In consideration of the response to ground-wind turbulence, it is indicated that the spatial correlation of gusts along the vehicle length can have significant effects. Finally, it is hoped that by correlation of response measurements now being obtained on full-scale vehicles with those predicted from models the adequacy of existing simulation techniques can be better established.

SYMBOLS

a_n, b_n	generalized coordinates for the nth modal functions in the x and y directions, respectively
C_L	lateral force coefficient
$C_{\dot{x}}$	aerodynamic damping coefficient
c	viscous damping coefficient
D	diameter
D_0	vehicle maximum diameter
f(r), g(r)	nondimensional correlation functions of velocity components parallel and perpendicular, respectively, to a line r between two points in the field of turbulence
f	frequency, cps
$F_S(t)$	random forcing function due to vortex shedding from a fixed cylinder
$F_D(t)$	aerodynamic damping force
H_i	frequency response functions relating response to a unit sinusoidal input force at station i on the structure
$H_n^{(1)}(i\alpha)$	Bessel function of the third kind
k	reduced frequency ($k = \omega D_0/U_0$), or spring constant
$K_n(\alpha)$	Bessel function of the second kind for imaginary argument
ℓ	vehicle over-all length
L	scale of turbulence (see eq. (A-8))
m	auxiliary damper mass or mass per unit length
M_n	generalized mass of the nth natural mode
M_x, M_y	bending moment about axis indicated by subscript
p_i, q_i	orthogonal components of gust velocity at a point i

$Q_{x,n}$ $Q_{y,n}$	generalized forces for the nth mode in x and y directions, respectively
r	correlation distance
R_e	real part of a complex quantity
$R_{ij}(\tau)$	cross correlation of horizontal gust components at point i and j on a vertical line
S_{n1}, S_{n2}, S_{n3}	integrals defined in appendix B
s	nondimensional time ($s = U_0 t/D_0$)
t, τ, T	time
T_{un}, T_{vn}	attenuation of response spectra in nth mode due to spatial correlation of u and v gusts (see eq. B-15))
u,v	horizontal components of turbulence in direction parallel and perpendicular, respectively, to the mean wind
u_0, v_0	amplitude of sinusoidal u and v gusts
U, U_0	mean wind velocity, subscript 0 denotes reference value
U_e	equivalent uniform wind velocity
W(z)	function defined in equation (B-4)
x,y	deflection response or horizontal axes
x_{st}	static deflection associated with mean wind
x_n, y_n	deflections of nth natural mode of vehicle relative to the tip deflection
z	axial distance along vehicle
$\alpha = \frac{\Delta z}{L}\sqrt{1+\nu^2}$	
γ	normalized cross spectra of gusts (see eqs. (A-15) and (A-17))
δ	see equation (B-3)
ϵ	distance between segmented areas

ζ	viscous damping ratio relative to critical damping
ξ_n, η_n	Nondimensional response functions $\left(\xi_n = \frac{x_n}{D_0},\ \eta_n = \frac{y_n}{D_0}\right)$
κ_n	density ratio parameter $\left(\kappa_n = \frac{\rho \ell D_0^2}{M_n}\right)$
κ	constant in figure 9 $\left(\kappa = \frac{\rho U^2 D}{2m}\right)$
λ	nondimensional time delay $\left(\lambda = \frac{U\tau}{L}\right)$
ν	reduced frequency based on L, $\left(\nu = \frac{\omega L}{U}\right)$
ρ	density of air or wind-tunnel test medium
σ	nondimensional separation distance $\left(\sigma = \frac{\Delta z}{L}\right)$ or standard deviation of a random variable
$\Phi_{ij}(\omega)$	power spectra or cross spectra of a random variable
ω	circular frequency

Notation:

A dot (•) denotes differentiation with respect to time

A prime (') denotes differentiation with respect to s

A bar (-) denotes average value

An asterisk (*) denotes conjugate of a complex quantity

Vertical bars || denote modulus of a complex quantity

$\lfloor\ \rfloor$ row matrix

$[\ ]$ square matrix

$\{\ \}$ column matrix

APPENDIX A

DERIVATION OF CROSS SPECTRA OF VERTICALLY SEPARATED COMPONENTS OF TURBULENCE

Consider the horizontal components of turbulence along a fixed vertical line representing the center line of an erected vehicle. In accordance with Taylor's hypothesis it will be assumed that turbulence can be treated as a space pattern of velocities which are transported at a mean horizontal velocity U. In addition, the turbulence is assumed to be homogeneous and locally isotropic. With these assumptions the correlation of velocities between two points depends only on the distance between the points so that a simple relationship exists between space correlations and time correlations.

The method of analysis to follow may be considered an extension of the cross spectra of vertical gust derived by Houbolt (ref. 24) in connection with two-dimensional gust loads on aircraft.

Cross Spectra of u(t)

Consider the u component of turbulence at two points a distance Δz apart on the vertical z axis (see sketch a).

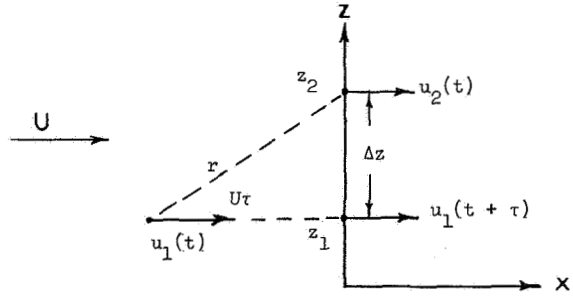

Sketch a.

The quantity of interest is the cross correlation between $u_1(t + \tau)$ and $u_2(t)$ from which the cross spectra can be derived. The cross correlation function, defined as

$$R_{12}(\tau) = \lim_{T \to \infty} \frac{1}{T} \int_0^T u_1(t)u_2(t + \tau)dt \qquad (A\text{-}1)$$

can be expressed in terms of the one-dimensional correlation function of the turbulence field. The two such functions required are $f(r)$ and $g(r)$ which denote the correlation of velocity components parallel and transverse, respectively, to a line r between two points in the field. (See sketch b.)

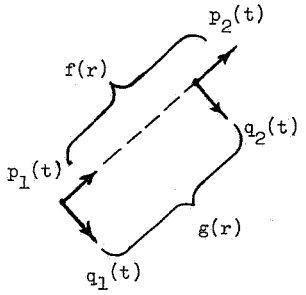

Consider the situation at time t. The velocity at point z_2 in sketch a is $u_2(t)$. Upstream of point z_1 a distance $U\tau$ is the velocity $u_1(t)$ which will arrive at z_1 τ seconds later. These components, $u_1(t + \tau)$ and $u_2(t)$, can be expressed in terms of components parallel and perpendicular to the line $r = \sqrt{(\Delta z)^2 + (U\tau)^2}$ at time t. Thus

$$u_1(t + \tau) = p_1(t) \cos \theta + q_1(t) \sin \theta$$

$$u_2(t) = p_2(t) \cos \theta + q_2(t) \sin \theta \qquad (A\text{-}2)$$

where

$$\sin\theta = \frac{\Delta z}{\sqrt{(\Delta z)^2 + U^2\tau^2}} \; ; \quad \cos\theta = \frac{U\tau}{\sqrt{(\Delta z)^2 + U^2\tau^2}}$$

Substitution of equation (A-2) into equation (A-1) yields

$$R_{12}(\tau) = \overline{u^2}\left[f(r)\cos^2\theta + g(r)\sin^2\theta\right] \tag{A-3}$$

where $f(r)$ is the correlation of velocities p_1 and p_2 in the direction of r and $g(r)$ is the correlation of velocities q_1 and q_2 in the direction normal to r. These correlations are defined as

Longitudinal:

$$f(r) = \frac{R_{p_{12}}(r)}{R_{p_{11}}(0)} = \frac{\overline{p_1 p_2}}{\overline{p_1^2}} \tag{A-4}$$

Transverse:

$$g(r) = \frac{R_{q_{12}}(r)}{R_{q_{11}}(0)} = \frac{\overline{q_1 q_2}}{\overline{q_1^2}}$$

Also, in deriving equation (A-3) use has been made of the following relations which result from the assumption of isotropic turbulence

$$\overline{p_1^2} = \overline{q_1^2} = \overline{u^2}$$

and

$$\overline{p_1 q_1} = \overline{p_2 q_2} = \overline{0} \tag{A-5}$$

The cross spectrum of the $u_1 u_2$ components of turbulence is defined as the Fourier transforms of the cross-correlation function given by equation (A-3)

$$\Phi_{12}(\omega) = \frac{1}{\pi} \int_{-\infty}^{\infty} R_{12}(\tau) e^{-i\omega\tau} \, dt \qquad \text{(A-6)}$$

Thus in order to derive a specific analytical expression for the cross spectrum it is necessary to assume a specific form of $f(r)$ and $g(r)$ in equation (A-3). For this purpose the simple exponential correlation functions which closely follows the form of isotropic turbulence observed in wind tunnels will be used. (See refs. 33 and 34.) These functions are

$$\left.\begin{aligned} f(r) &= e^{-|r|/L} \\ g(r) &= \left[1 - \frac{|r|}{2L}\right] e^{-|r|/L} \end{aligned}\right\} \qquad \text{(A-7)}$$

where L is the so-called integral - scale of turbulence defined as

$$L = \int_0^{\infty} f(r) \, dr \qquad \text{(A-8)}$$

Substitution of equations (A-7) into equation (A-3) gives

$$R_{12}(\tau) = \frac{\overline{u^2}}{(\Delta z)^2 + U^2\tau^2} \left[U^2\tau^2 e^{-\frac{\sqrt{(\Delta z)^2+U^2\tau^2}}{L}} + (\Delta z)^2 \left(1 - \frac{\sqrt{(\Delta z)^2 + U^2\tau^2}}{2L}\right) e^{-\frac{\sqrt{(\Delta z)^2+U^2\tau^2}}{L}} \right] \qquad \text{(A-9)}$$

Now let

$$\sigma = \Delta z/L$$

$$\lambda = U\tau/L$$

Then

$$R_{12}(\lambda) = \overline{u^2}\left(1 - \frac{\sigma^2}{2\sqrt{\sigma^2 + \lambda^2}}\right) e^{-\sqrt{\sigma^2+\lambda^2}} \qquad \text{(A-10)}$$

and the cross spectra of turbulence then follows from equation (A-6)

$$\left.\begin{aligned} \Phi_{u_{12}}(\omega) &= \frac{\overline{u^2}L}{\pi U} \int_{-\infty}^{\infty} \left(1 - \frac{\sigma^2}{2\sqrt{\sigma^2 + \lambda^2}}\right) e^{-\sqrt{\sigma^2+\lambda^2}} e^{-i\omega\tau} d\tau \\ \text{or} \\ \Phi_{u_{12}}(\nu) &= \frac{\overline{u^2}}{\pi} \int_{-\infty}^{\infty} \left(1 - \frac{\sigma^2}{2\sqrt{\sigma^2 + \lambda^2}}\right) e^{-\sqrt{\sigma^2+\lambda^2}} e^{-i\omega\lambda} d\lambda \end{aligned}\right\} \qquad \text{(A-11)}$$

where $\nu = \omega L/U$. Integration of this equation produces the following expression for cross spectrum

$$\left.\begin{aligned} \Phi_{u_{12}}(\nu) &= \frac{2\overline{u^2}\sigma^2}{\pi}\left[\frac{1}{\alpha} K_1(\alpha) - \frac{1}{2} K_0(\alpha)\right] \\ &= \frac{\overline{u^2}\sigma^2}{2}\left[-\frac{2}{\alpha} H_1^{(1)}(i\alpha) - iH_0^{(1)}(i\alpha)\right] \end{aligned}\right\} \qquad \text{(A-12)}$$

where

$$\alpha = \sigma\sqrt{1 + \nu^2}$$

and

$K_n(\alpha)$ the Bessel function of the second kind for imaginary argument,

$H_n^{(1)}(i\alpha)$ the Bessel function of the third kind

Equation (A-12) is a real quantity indicating that the derived cross spectrum has a zero quadrature component.

As the separation distance Δz approaches zero, the cross spectrum (eq. (A-12)) reduces to the power spectrum of the u component of turbulence which, for $f(r) = e^{-r/L}$, is simply

$$\Phi_{u_{11}}(\nu) = \frac{\overline{2u^2}}{\pi} \frac{1}{1 + \nu^2} \tag{A-13}$$

It is convenient in response calculations to express the cross spectrum in the following normalized form

$$\gamma_{u_{12}} = \frac{\Phi_{u_{12}}}{\Phi_{u_{11}}} \tag{A-14}$$

Equations (A-12) and (A-13) substituted into equation (A-14) give

$$\gamma_{u_{12}} = \frac{\pi}{4} \alpha \left[-2H_1^{(1)}(i\alpha) - \alpha H_0^{(1)}(i\alpha) \right] \tag{A-15}$$

An important simplification results when it is recognized that the wavelengths for frequencies of primary interest are in general less than the scale of turbulence; that is $2\pi(U)/\omega < L$. The parameter α in equation (A-15) then reduces to a single nondimensional parameter

$$\alpha = \frac{\Delta z}{L} \sqrt{1 + \frac{\omega L}{U}^2}$$

$$\approx \frac{\omega \Delta z}{U} \quad \text{for} \quad \frac{\omega L}{U} >> 1.0 \tag{A-16}$$

Therefore

$$\gamma_{u_{12}} \approx \frac{\pi}{4}\left(\frac{\omega\,\Delta z}{U}\right)\left[-2H_1^{(1)}\left(i\,\frac{\Delta z\omega}{U}\right)-\frac{\omega\Delta z}{U}H_0^{(1)}\left(i\,\frac{\omega\Delta z}{U}\right)\right] \qquad \text{(A-17)}$$

The absolute value of equation (A-17) is shown plotted in figure 15(a), together with experimental data obtained by Singer in reference 30 and Davenport in reference 29.

Cross Spectra of v(t)

The equation for the cross spectra of horizontal transverse v components of turbulence is identical to Houbolt's expression for the vertical w components presented in reference 24. This expression is

$$\Phi_{v_{12}}(\nu) = \frac{\overline{u^2}}{2}\left\{\frac{-\sigma^2}{1+\nu^2}\left[iH_0^{(1)}(i\alpha)\right] + \frac{\sigma(1+3\nu^2)}{(1+\nu^2)^{3/2}}\left[-H_1^{(1)}(i\alpha)\right]\right\} \qquad \text{(A-18)}$$

In the limit for $\Delta z = \sigma = 0$, this equation reduces to the power spectrum for transverse components of turbulence which, for $g(r)$ as given in equation (A-7), is

$$\Phi_{v_{11}}(\nu) = \frac{\overline{u^2}}{\pi}\frac{1+3\nu^2}{(1+\nu^2)^2} \qquad \text{(A-19)}$$

Therefore

$$\gamma_{v_{12}} = \frac{\Phi_{v_{12}}}{\Phi_{v_{11}}} = \frac{\pi}{2}\left\{\frac{-\alpha^2}{1+3\nu^2}\left[iH_0^{(1)}(i\alpha)\right] - \alpha\left[H_1^{(1)}(i\alpha)\right]\right\} \qquad \text{(A-20)}$$

Again, it can be stated that for the frequency range of interest in the present study ($\nu >> 1.0$) equation (A-20) is essentially a function of $\omega\ \Delta z/U$ alone and can be written

$$\gamma_{v_{12}} \approx \frac{\pi}{2} \frac{\omega\ \Delta z}{U} H_1^{(1)}\left(i\ \frac{\Delta z \omega}{U} \right) \tag{A-21}$$

Equation (A-21) is found to be an excellent approximation to equation (A-20) for wavelengths equal to or less than $2L$.

A plot of equation (A-21) as a function of $f\ \Delta z/U$ is shown in figure 15(b), where f is frequency in cycles per second.

In order to obtain somewhat simpler analytical expressions for use in response calculations, the cross spectra defined by equations (A-15) and (A-21) have been approximated by damped cosine functions. On the basis of a least-squares-fit, the following empirical equations were obtained.

$$\left.\begin{aligned} \gamma_{u_{12}} &= e^{-4.4(f\ \Delta z)/U} \cos \frac{4\pi}{3}\left(\frac{f\ \Delta z}{U} \right) \\ \text{and} \qquad \gamma_{v_{12}} &= e^{-3.2(f\ \Delta z)/U} \cos \frac{\pi}{2}\left(\frac{f\ \Delta z}{U} \right) \end{aligned}\right\} \tag{A-22}$$

APPENDIX B

DERIVATION OF GUST RESPONSE EQUATIONS

Frequency Response Functions

Two sets of frequency response functions will be derived. One set relates the response of the vehicle in the x direction to a sinusoidal $u(t)$ gust input and the other relates response in the y direction to a sinusoidal $v(t)$ gust input. The following assumptions are made:

a. The vehicle is structurally and aerodynamically symmetrical about its z axis which is vertical.

b. Wind forces on the vehicle are proportional to the local diameter such that the assumptions of two-dimensional strip theory are applicable.

c. Wind forces are quasi-static (proportional to the instantaneous dynamic pressure) and act in the direction of flow relative to the vehicle.

d. The unsteady components of wind are small in relation to the mean wind speed.

e. Coupling between natural structural modes can be neglected.

First, consider the deflection response of a vehicle in the direction of the mean wind. Let the x component of deflection be expressed in terms of natural modes of the structure

$$x(z,t) = a_1(t)x_1(z) + a_2(t)x_2(z) + \ldots \tag{B-1}$$

where $x_n(z)$ is the nth natural mode shape and $a_n(t)$ is a generalized coordinate determined from solution of the differential equation

$$\ddot{a}_n + 2\zeta_n \omega_n \dot{a}_n + \omega_n{}^2 a_n = \frac{Q_{x,n}}{M_n} \tag{B-2}$$

In equation (B-2) ζ_n is the equivalent viscous structural damping relative to critical damping, ω_n the natural frequency, M_n the generalized mass, and $Q_{x,n}$ the generalized force – each for nth mode of vibration.

Assume that a gust velocity $u(t)$ acts over an element of length ε centered over station z_1 on the structure. The generalized force in equation (B-2) then becomes

$$Q_{x,n} = \int_0^{l} \frac{1}{2} \rho C_D D \left[U - \dot{a}_n x_n + u(t)\delta(z,z_1) \right]^2 x_n dz \qquad \text{(B-3)}$$

where $\delta(z,z_1)$ is a function which has the following properties

$$\delta(z,z_1) = 1 \quad \text{when} \quad (z_1 - \frac{\varepsilon}{2}) \leq z \leq (z_1 + \frac{\varepsilon}{2})$$

$$= 0 \text{ elsewhere}$$

With the assumption that the air density ρ is constant and the mean wind U is large compared with u and $\dot{a}_n$, equation (B-3) can be written

$$Q_{x,n} = \frac{1}{2} \rho U_0^2 D_0 l \left[S_{1n} - 2 \frac{\dot{a}_n}{U_0} S_{2n} + 2 \frac{\varepsilon}{l} W(z_1) \frac{u(z_1, t)}{U_0} \right] \qquad \text{(B-4)}$$

where

$$W_n(z) = \frac{D(z)}{D_0} \frac{U(z)}{D_0} x_n(z) C_D(z)$$

$$S_{n1} = \int_0^1 W_n \frac{U}{U_0} d\left(\frac{z}{l}\right)$$

$$S_{n2} = \int_0^1 W_n x_n d\left(\frac{z}{l}\right)$$

With the notation

$$\xi_n = \frac{a_n}{D_0}$$

$$\frac{\partial}{\partial t} = \frac{U_0}{D_0}\frac{\partial}{\partial s}$$

equation (B-2) becomes

$$\xi_n'' + (2\zeta_n k_n + \kappa S_{n2})\xi_n' + k_n^2 \xi_n = \kappa\left[\frac{1}{2}S_{n1} + \frac{\varepsilon}{l}W(z_1)\frac{u(z_1,t)}{U_0}\right] \quad \text{(B-5)}$$

where $k_n = \dfrac{\omega_n D_0}{U_0}$

$$\kappa_n = \frac{\rho l D^2}{M_n}$$

and a prime denotes, $\dfrac{\partial}{\partial s}$.

If the gust at z_1 is assumed to vary sinusoidally with time in equation (B-5); that is, $u_n(z_1,t) = u_{n0}e^{iks}$, $\xi_n = \xi_{n0}e^{iks}$, then the frequency response function for dynamic deflections of a vehicle in the x direction associated with this gust input is

$$H_{\xi_n 1}(k) = \frac{\xi_{n0}}{\frac{u_{n0}}{U_0}} = \frac{\kappa\frac{\varepsilon}{l}W_n(z_1)}{k_n^2 - k^2 + i(2\zeta_n k_n + \kappa S_{n2})k} \quad \text{(B-6)}$$

Note that the static dragwise deflection has been subtracted from the total deflection in obtaining equation (B-6).

The response of the vehicle in the direction transverse to the wind can be similarly expressed in terms of natural modes

$$y(z,t) = b_1(t)y_1(z) + b_2(t)y_2(z) + \ldots \tag{B-7}$$

where b_n is determined from the equation

$$\ddot{b}_n + 2\zeta_n\omega_n\dot{b}_n + \omega_n^2 b_n = \frac{Q_{y,n}}{M_n} \tag{B-8}$$

and $y_n(z) = x_n(z)$ by symmetry. The generalized force for transverse response is

$$Q_{y,n} = \int_0^{\ell} \frac{1}{2}\rho C_D D \left\{ U^2 + \left[-\dot{b}_n y_n + v(t)\delta(z,z_1) \right]^2 \right\} y_n \sin\beta dz \tag{B-9}$$

where

$$\sin\beta = \frac{-\dot{b}y_n + v\delta(z,z_1)}{\sqrt{U^2 + \left[-\dot{b}_n y_n + v\delta(z,z_1) \right]^2}}$$

In a manner similar to that followed in obtaining equation (B-6) the frequency response function for the transverse response becomes

$$H_{\eta_n 1}(k) = \frac{\frac{\eta_{n0}}{D_0}}{\frac{v_{n0}}{U_0}} = \frac{0.5\,\kappa_n \frac{\varepsilon}{\ell} W_n(z_1)}{k_n^2 - k^2 + i\left(2\zeta_n k_n + 0.5\,\kappa S_{n2}\right)k} \tag{B-10}$$

where $\eta_n = \frac{b_n}{D_0}$.

For cases wherein the gust input is assumed to be perfectly correlated along the length of a vehicle the frequency response functions may be obtained by

integrating equations (B-6) and (B-10) over the vehicle length. Thus for a uniformly distributed $u(t)$ gust the frequency response function for deflection in the x direction is from equation (B-6)

$$H_{\xi_n}(k)\Big|_{\text{uniform}} = \frac{\kappa_n S_{n3}}{k_n^2 - k^2 + i(2\zeta_n k_n + \kappa S_{n2})k} \tag{B-11}$$

and similarly for a uniformly distributed $v(t)$ gust in equation (B-10)

$$H_{\eta_n}(k)\Big|_{\text{uniform}} = \frac{0.5\kappa_n S_{n3}}{k_n^2 - k^2 + i(2\zeta_n k_n + 0.5\kappa S_{n2})k} \tag{B-12}$$

where $S_{n_3} = \int_0^1 W_n(z)\,d(z/l)$.

Response Spectrum

With the turbulence spectra relationships in appendix A and the frequency response functions derived in the previous section, working equations for the structural response spectrum for the nth mode can be formulated as follows:

For a uniform one-dimensional gust input equations (3), (B-11), and (B-12) combine to yield

one-dimensional u gust

$$\Phi_{\xi}(k)_{n,\ \text{uniform}} = \frac{\kappa_n^2 S_{n3}^2}{\left(k_n^2 - k^2\right)^2 + \left(2\zeta_n k_n + \kappa_n S_{n2}\right)^2 k^2} \Phi_{u/U_0}(k) \tag{B-13a}$$

one-dimensional v gust

$$\Phi_{\eta}(k)_{n,\ \text{uniform}} = \frac{0.25\kappa_n{}^2 S_{n3}{}^2}{\left(k_n{}^2 - k^2\right)^2 + \left(2\zeta_n k_n + 0.5\kappa_n S_{n2}\right)^2 k^2} \Phi_{v/U_0}(k) \qquad \text{(B-13b)}$$

The turbulence spectra in these equations are expressed as a function of $k = \frac{\omega D_0}{U_0}$ and u and v are normalized with respect to U_0. With these changes in variables the spectra given by equation (A-13) and equation (A-19) become, respectively

$$\Phi_{u/U_0}(k) = \frac{2}{\pi} \frac{\overline{u^2}}{U_0{}^2} \frac{L/D_0}{1 + (L/D_0)^2 k^2} \qquad \text{(B-14a)}$$

$$\Phi_{v/U_0}(k) = \frac{2}{\pi} \frac{\overline{v^2}}{U_0} \frac{L}{D_0} \frac{1 + 3(L/D_0)^2 k^2}{\left[1 + (L/D_0)^2 k^2\right]^2} \qquad \text{(B-14b)}$$

For two-dimensional gust inputs the following expressions can be derived

two-dimensional u gust

$$\Phi_{\xi_n}(k) = T_{un}(k)\Phi_{\xi}(k)_{n,\ \text{uniform}} \qquad \text{(B-15a)}$$

two-dimensional v gust

$$\Phi_{\eta_n}(k) = T_{vn}(k)\Phi_{\eta}(k)_{n,\ \text{uniform}} \qquad \text{(B-15b)}$$

where the functions $T_{un}(k)$ and $T_{vn}(k)$ are in the nature of "attenuation" factors which account for the two-dimensionality of the gust field. These "attenuation" factors can be expressed in matrix notation as follows:

$$T_n(k) = \frac{(\varepsilon/L)^2}{S_{nl}^2} \left[W_n(j\varepsilon)\right] \left[\gamma_{ij}(k)\right] \left\{W_n(j\varepsilon)\right\} \qquad \text{(B-16)}$$

where

$i = 1, 2, \ldots m$

$j = 1, 2, \ldots m$

The elements $\gamma_{ij}(k)$, representing the real part of the normalized cross spectrum between points i and j, are given for the u and v components of turbulence by the approximate formulas in equation (A-22). This function depends on the properties of turbulence and is independent of structural parameters. The quantity $W(j\varepsilon)$, on the other hand, depends on the diameter and mode shape of the structure as well as the shape of the mean wind profile. (See eq. (B-4).)

1. Pagon, W. Watters: Vibration Problem in Tall Stacks Solved by Aerodynamics. Engineering News Record, July 12, 1934.

2. Maher, F. J., Frederick, D., Estes, E. R., and Steinman, D. B.: Wind-Tunnel Tests of Suspension Bridge Section Models. Bull. Virginia Polytechnic Institute, Eng. Exp. Station, Series No. 69, Vol. 41, No. 6, 1948, pp. 1-50.

3. Den Hartog, J. P.: Recent Technical Manifestations of von Karman's Vortex Wake. Proc. Nat. Acad. Sci. of USA, Vol. 40, 1954, pp. 155-157.

4. Boorne, R. A.: The Aeroelastics of Tall Stacks. Inst. Aero. Sci., Preprint No. 851, Oct. 1958.

5. Goldman, R.: The Generation and Suppression of von Karman Vortex Forces. Martin Co. Eng. Report No. 8984, July 1957.

6. Buell, Donald A., and Kenyon, George C.: The Wind-Induced Loads on a Dynamically Scaled Model of a Large Missile in Launching Position. NASA TM X-109, December 1959.

7. Young, J. P.: Wind-Induced Oscillation Tests of 1/6-Scale Pershing Model. The Martin Company Engineering Report No. 11461, August 1960.

8. Killough, T. L.: Wind-Induced Loads on a Dynamic 1/5-Scale Unfueled SM-78 Jupiter in the Launch Position (U), U. S. Army Ordnance Missile Command, Report No. RG-TM-62-65, July 10, 1962.

9. Cincotta, J. J., and Lambert, W. H.: Investigation of Wind Induced Oscillations and Steady Ground Wind Forces on a 7 1/2% Dynamically Scaled Model of the 624A Vehicle (U). The Martin Company, May 1963. Contract No. ER 13022

10. Fung, Y. C.: Fluctuating Lift and Drag Acting on a Cylinder in a Flow at Supercritical Reynolds Numbers. Jour. Aerospace Sciences, Vol. 27, No. 11, pp. 801-804, Nov. 1960.

11. Humphreys, J. S.: On a Circular Cylinder in a Steady Wind. Jour. of Fluid Mechanics, Vol. 9, Pt. 4, Dec. 1960, p. 603.

12. Buell, Donald A., McCullough, George B., and Steinmetz, William J.: A Wind-Tunnel Investigation of Ground-Wind Loads on Axisymmetric Launch Vehicles. NASA TN D-1893, October 1963.

13. Roshko, Anatol: Experiments of the Flow Past Circular Cylinders at Very High Reynolds Number. Jour. of Fluid Mechanics, Vol. 10, 1961.

14. Regier, Arthur A.: The Use of Scaled Dynamic Models in Several Aerospace Vehicle Studies. Proceedings ASME Winter Annual Meeting, Philadelphia, Pa., November 1963, pp. 34-50.

15. Hanson, Perry W., and Jones, George W., Jr.: On the Use of Dynamic Models for Studying Launch Vehicle Buffet and Ground-Wind Loads. Proceedings of Symposium on Aeroelastic and Dynamic Modeling Technology. RTD-TDR-63-4197, Part I, Dayton, Ohio, Sept. 23-25, 1963, pp. 333-387.

16. O'Neill, P. G. G.: Experiments to Simulate a Natural Wind Velocity Gradient in the Compressed Air Tunnel. NPL Aero Note 313, 1956.

17. Owen, P. R., and Zienkiewicz, H. K.: The Production of Uniform Shear Flow in A Wind Tunnel. Jour. of Fluid Mech., Vol. 2, Pt. 6, Aug. 1957, pp. 521-531.

18. Nemoto, S.: Similarity Between Natural Wind in the Atmosphere and Model Wind in a Wind Tunnel, Part III - Some Examples of Experiments. Meteorological Research Institute, Vol. 12, No. 2, 1961, Tokyo, pp. 129-154.

19. Den Hartog, J. P.: Mechanical Vibrations, 3rd Edition, McGraw-Hill, New York, 1947.

20. Woodgate, L.: Aerodynamic Stability Tests of a Model of a 250-Foot Steel Stack. NPL/Aero/408, National Physical Laboratory, Department of Scientific and Industrial Research, July 1960.

21. Ezra, A. A., and Birnbaum, S.: Design Criteria for Space Vehicles to Resist Wind-Induced Oscillations. American Rocket Soc. Paper 1081-60, Presented at the Struct. Design of Space Vehicles Conf., Santa Barbara, Calif., April 6-8, 1960.

22. Scruton, C.: On the Wind-Excited Oscillations of Stacks, Towers, and Masts. National Physical Laboratory, Paper 16, June 1963.

23. Houbolt, John C., Steiner, Roy, and Pratt, Kermit G.: Dynamic Response of Airplanes to Atmospheric Turbulence Including Flight Data on Input Response. NASA Technical Report R-199, 1964.

24. Houbolt, John C.: On the Response of Structures Having Multiple Random Inputs. Jahr. 1957 der WGL, Friedr. Vieweg and Sohn (Brauchschweig), pp. 296-305.

25. Bohne, Q. R.: Power Spectral Considerations on the Launch Pad. USAF Geophysics Res. Dir. A. F. Surveys in Geophysics., No. 140, Proc. of National Symposium on Winds for Aerospace Vehicle Design, Vol. 1, AFCRL-62-273(I), March 1962.

26. Henry, R. M., A Study of the Effects of Wind Speed Lapse Rate, and Altitude on the Spectrum of Atmospheric Turbulence at Low Altitude. IAS Preprint No. 59-43, Jan. 1959.

27. Davenport, A. G.: The Spectrum of Horizontal Gustiness Near the Ground in High Winds. Quarterly Jour. of Mat. Soc., Vol. 87, 1961.

28. Panofsky, H. A.: Surface Properties of Turbulence in the Boundary Layer. Unpublished report prepared for MSFC, Jan. 1964.

29. Davenport, Alan G.: The Response of Slender, Line-Like Structures to a Gusty Wind. Proc. Inst. Civil Engineers, 23: pp. 389-408.

30. Singer, Irving A.: A Study of the Wind Profile in the Lowest 400 Feet of the Atmosphere. Progress Reports No. 5 and 9, 1960-61, Brookhaven National Lab.

31. Daniels, Glenn E.: Terrestrial Environment (Climactic) Criteria Guidelines for Use in Space Vehicle Development, 1964 Revision. NASA TM X053023, Mar. 13, 1964, George C. Marshall Space Flight Center, Huntsville, Ala.

32. Reed. W. H., III, and Lynch, J. W.: A Simple Fast Response Anemometer. Jour. Applied Meteorology, Vol. 2, June 1963.

33. Dryden, H. L.: Turbulence Investigations at the National Bureau of Standards. Proc. Fifth International Congress of Applied Mechanics, Cambridge, 1938.

34. Liepmann, H. W., Laufer, J., and Liepmann, K.: On the Spectrum of Isotropic Turbulence. NACA TN No. 2473, 1951.

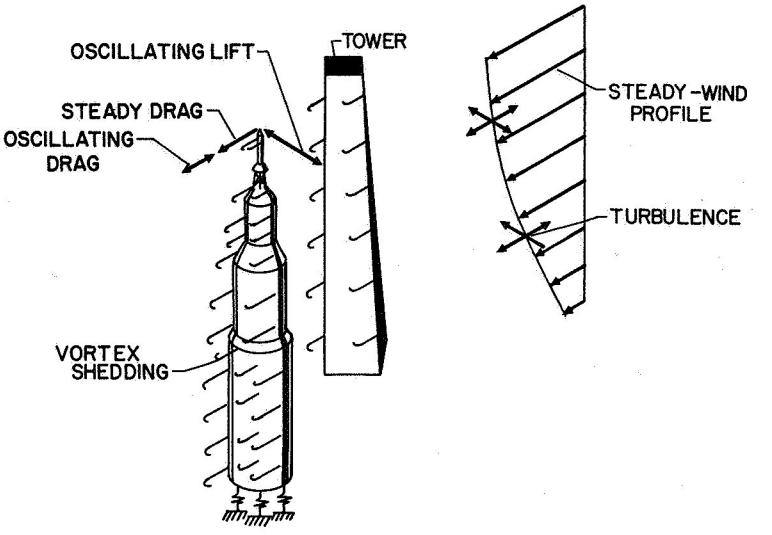

NASA

Figure 1.- Factors contributing to ground-wind loads.

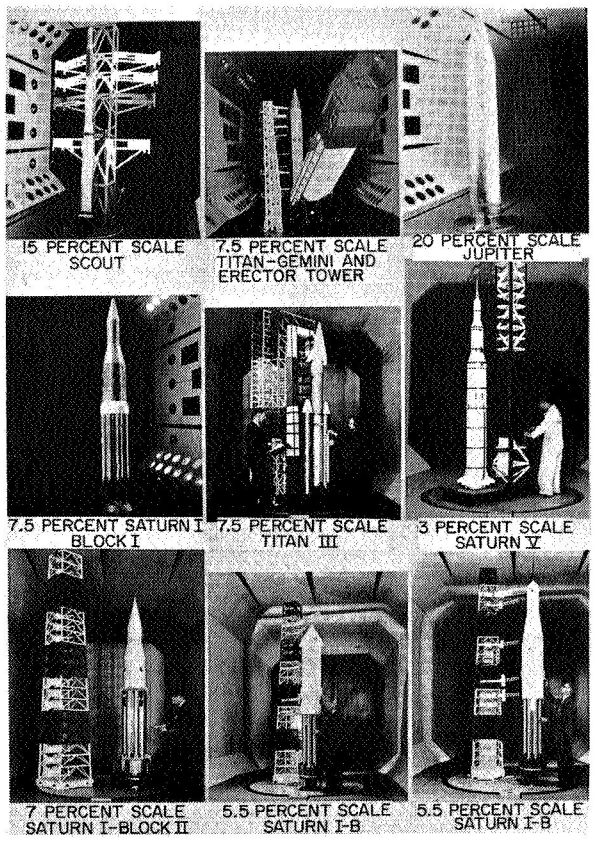

NASA

Figure 2.- Aeroelastic ground-wind-load models in the 16-foot Langley Transonic Dynamics tunnel.

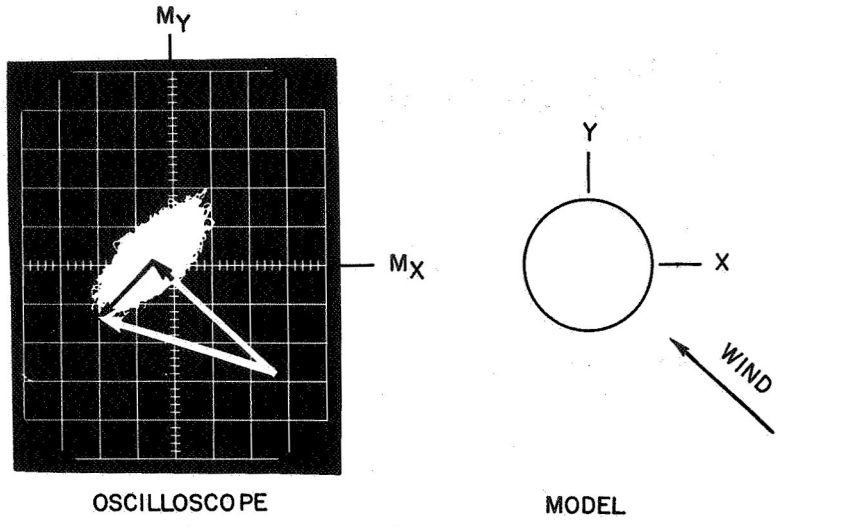

NASA

Figure 3.- Time exposure of bending moments on an oscilloscope screen.

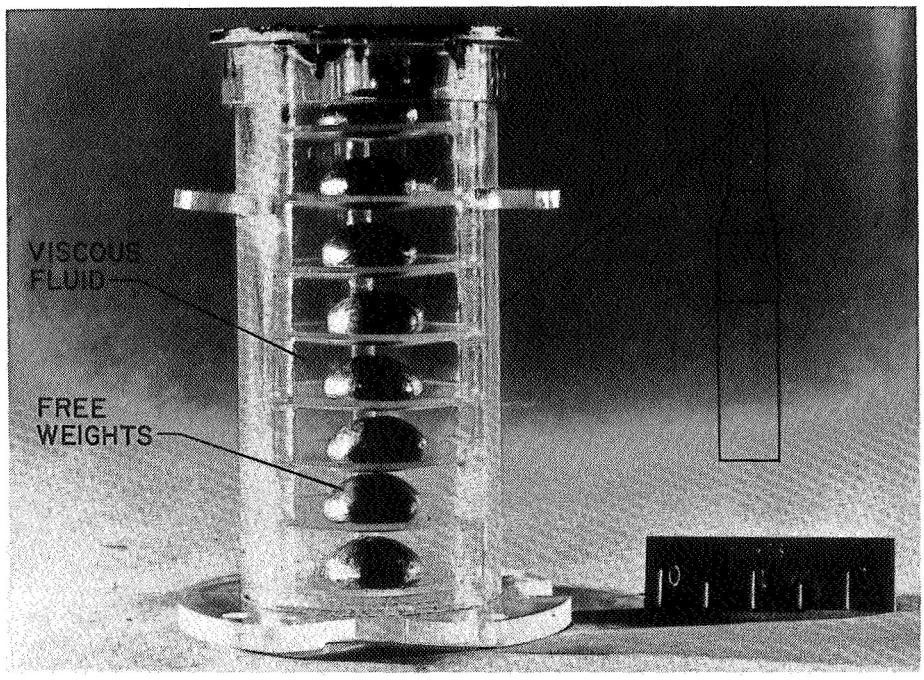

NASA

Figure 4.- Viscous damper used in ground-wind-load models.

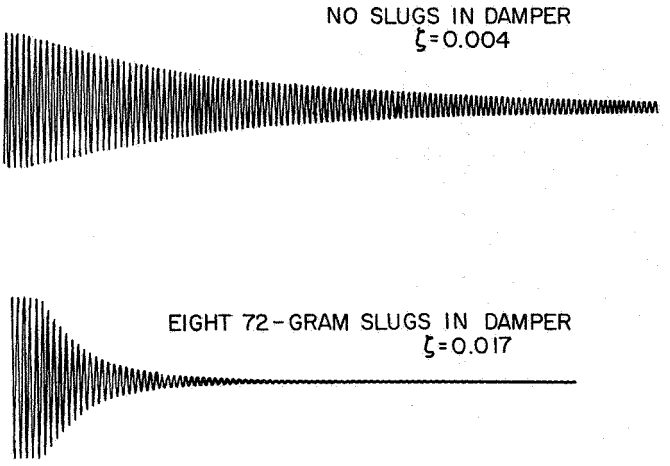

NASA

Figure 5.- Typical free-vibration records from 0.30-scale Saturn V model with and without slugs in damper.

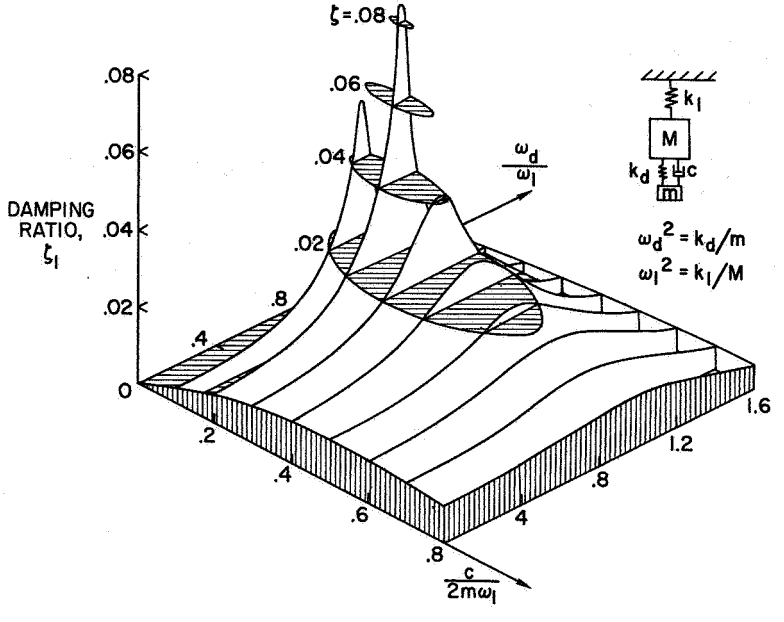

NASA

Figure 6.- Performance characteristics of an auxiliary mass damper. m/M = 0.05.

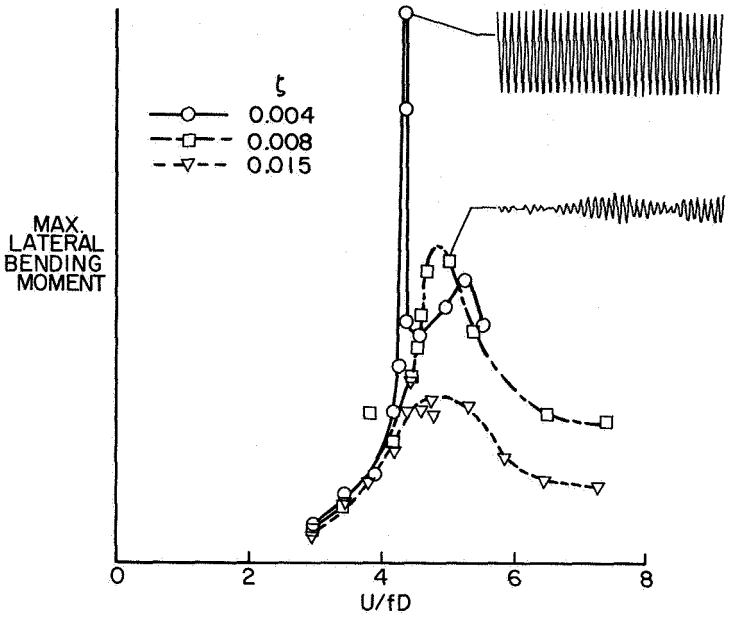

NASA

Figure 7.- Effect of damping on maximum dynamic bending moment response of 0.03-scale Saturn V model.

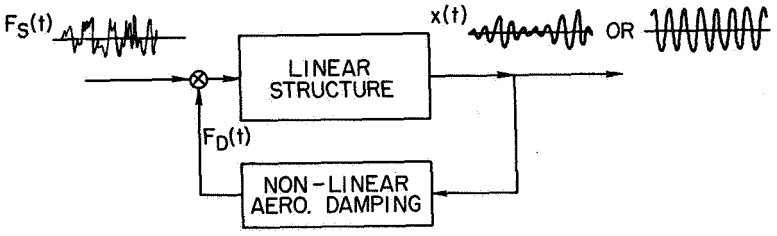

EQ. OF MOTION:

$$\ddot{x} + 2\zeta\omega_n\dot{x} + \omega_n^2 x = \frac{1}{m}\left[F_S(t) + F_D(t)\right]$$

$$= \frac{\rho U^2 D}{2m}\left[C_L(t) - C_{\dot{x}}\ \frac{\dot{x}}{U}\right]$$

NASA

Figure 8.- A conceptual representation of dynamic response of structures to wind-induced loads.

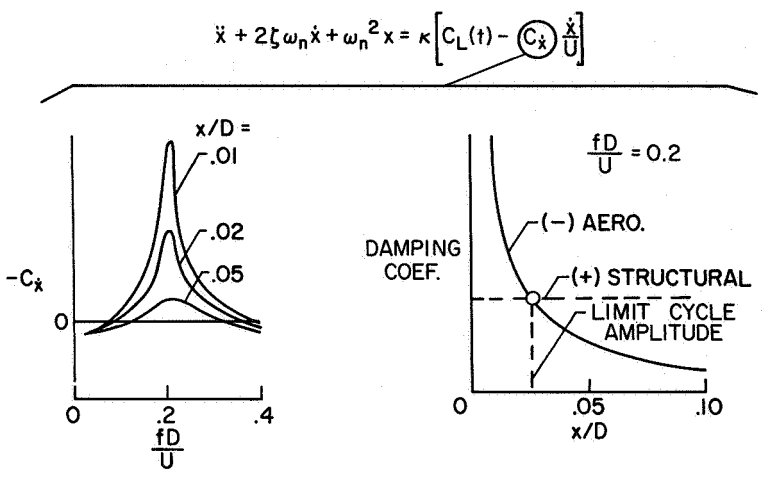

NASA

Figure 9.- Nonlinear aerodynamic characteristics associated with vortex shedding.

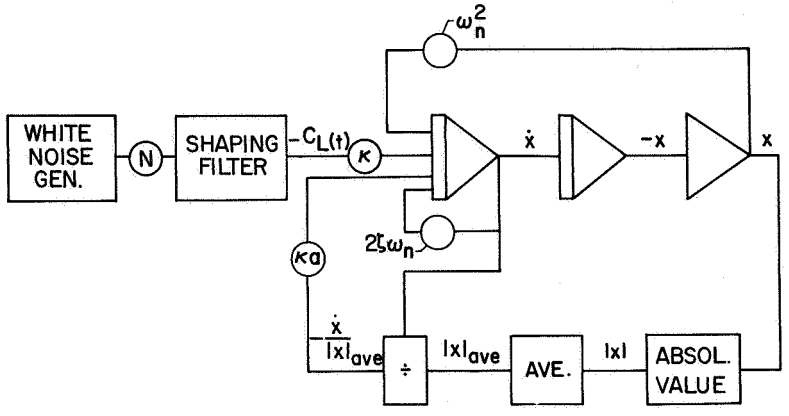

$$\ddot{x} + 2\zeta\omega_n\dot{x} + \omega_n^2 x = \kappa\left[C_L(t) + \frac{a}{|x|_{ave}}\dot{x}\right]$$

NASA

Figure 10.- Analog computer simulation of vortex-shedding phenomenon.

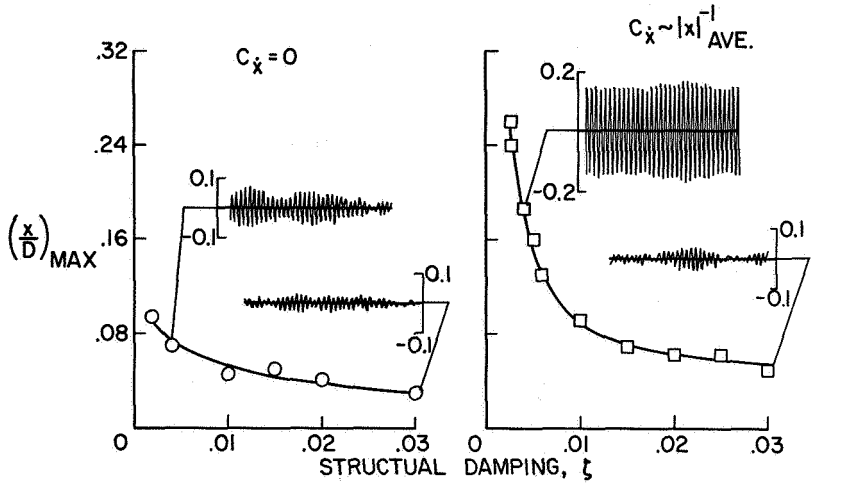

NASA

Figure 11.- Analog computer solutions showing effect of nonlinear aerodynamic damping on dynamic response.

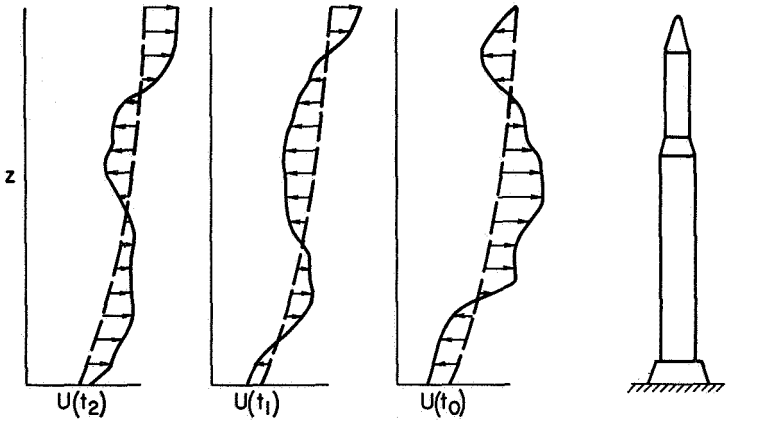

NASA

Figure 12.- Typical variations of unsteady wind with height.

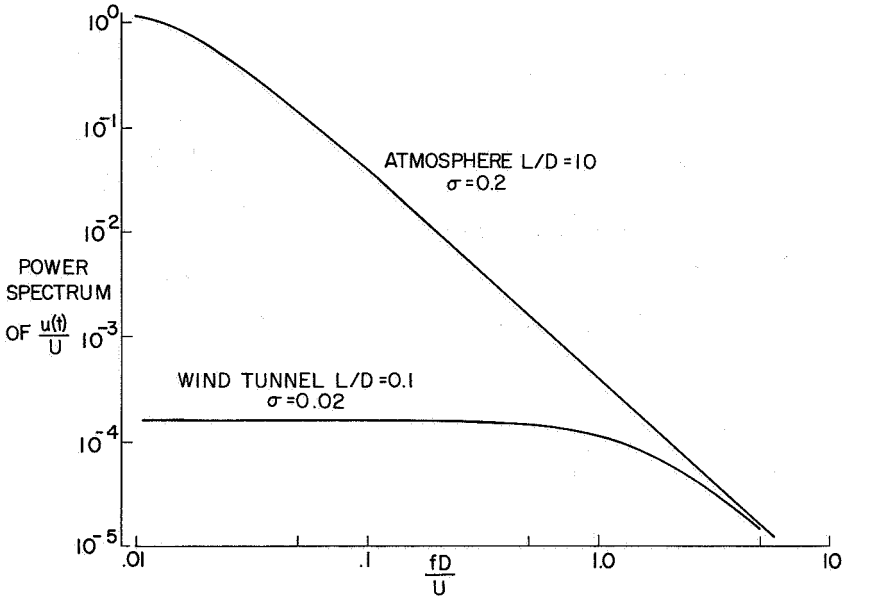

Figure 13.- Comparison of turbulence characteristics in wind tunnels and the atmosphere.

- ONE-DIMENSIONAL INPUT

$$\Phi_r(\omega) = |H(\omega)|^2 \Phi_u(\omega)$$

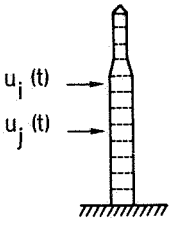

- TWO-DIMENSIONAL INPUT

$$\Phi_r(\omega) = \Phi_u(\omega) \left\{ H_1 H_1^* + H_2 H_2^* + \ldots + 2R_e \left[\frac{\Phi_{12}}{\Phi_u} \left(H_1^* H_2 + H_2^* H_3 + \ldots \right) + \frac{\Phi_{13}}{\Phi_u} \left(H_1^* H_3 + H_2^* H_3 + \ldots \right) + \ldots \frac{\Phi_{1n}}{\Phi_u} \left(H_1^* H_n + H_2^* H_{n+1} + \ldots \right) \right] \right\}$$

NASA

Figure 14.- Response equations for systems excited by multiple-random inputs.

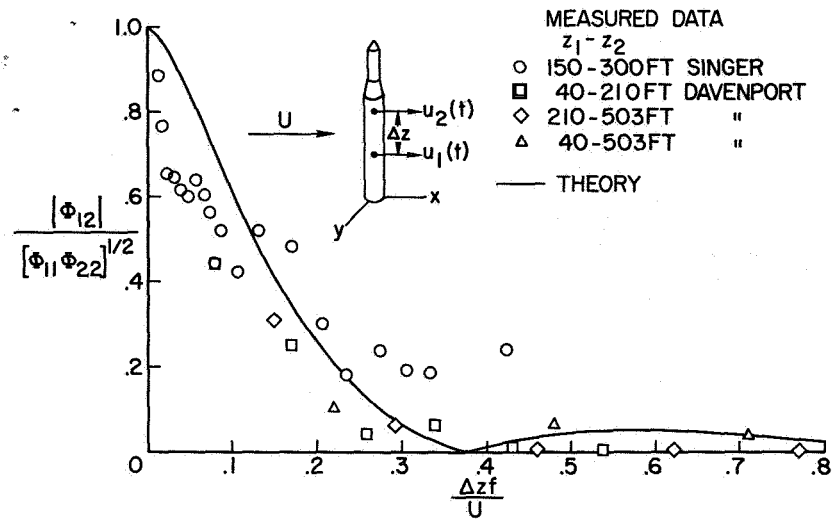

(a) u component.

NASA

Figure 15.- Cross spectra of turbulence components as a function of vertical separation distance.

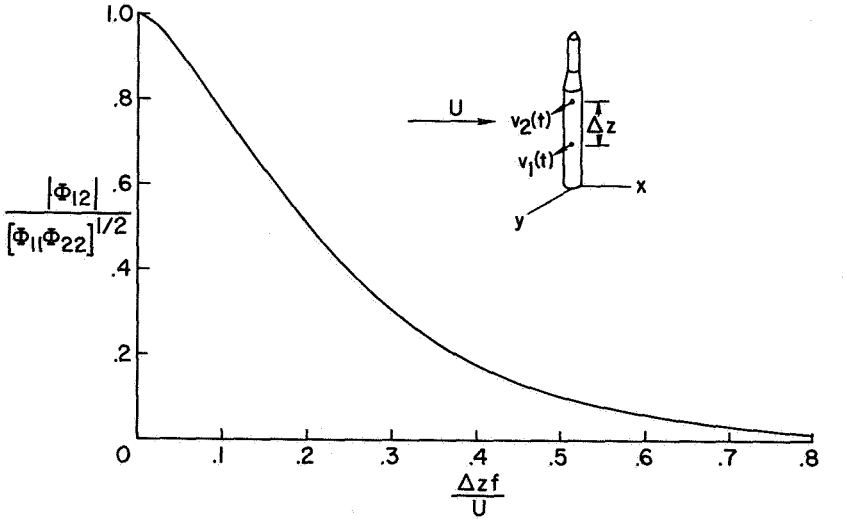

(b) v component.

NASA

Figure 15.- Concluded.

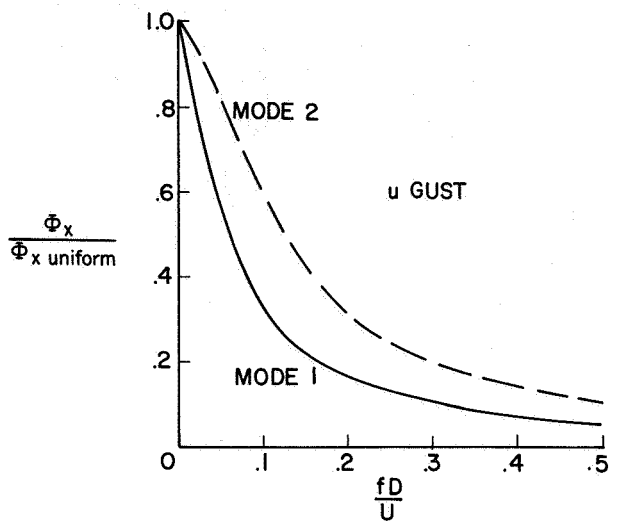

NASA

Figure 16.- Effect of gust correlation on modal response of a launch vehicle.

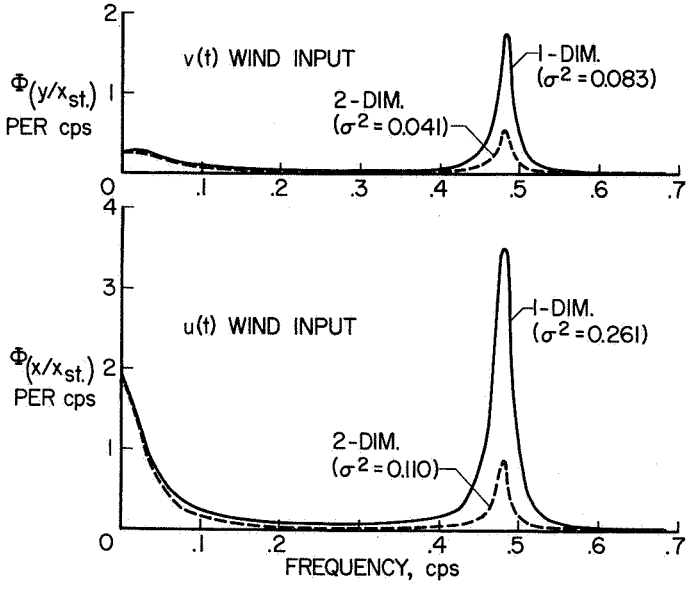

NASA

Figure 17.- Power spectrum of vehicle response to atmospheric turbulence.

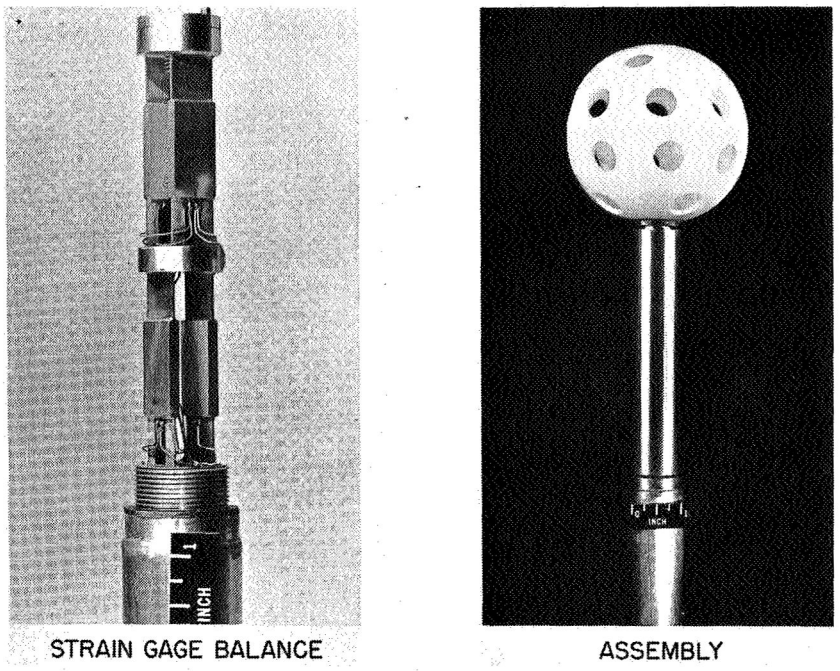

Figure 18.- Fast response anemometer.

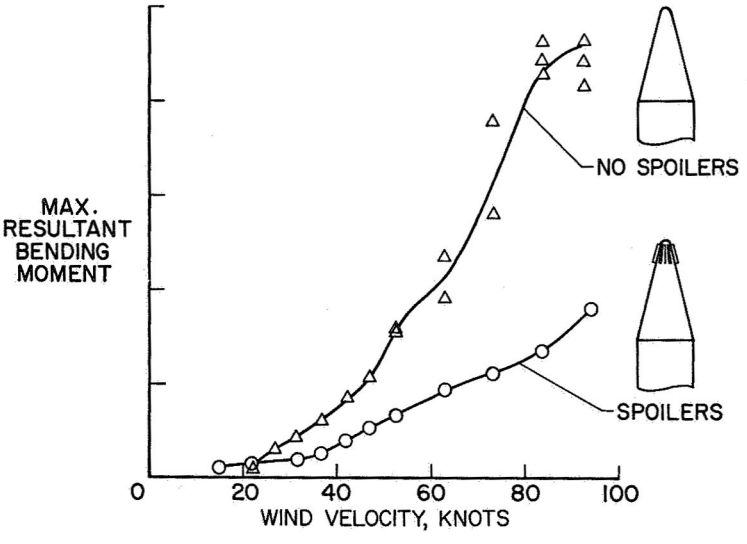

Figure 19.- Effect of nose spoilers on bending moment response of 0.20-scale Jupiter model.

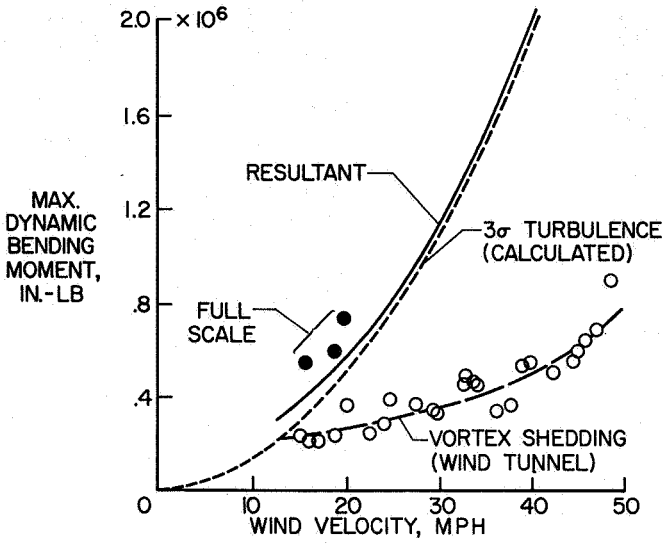

NASA

Figure 20.- Response of Titan-Gemini to ground-wind loads.